

The depolarisation properties of powerful extragalactic radio sources as a function of cosmic epoch

J.A. Goodlet^{*} & C. R. Kaiser

School of Physics & Astronomy, University of Southampton, Southampton SO17 1BJ

24 November 2018

ABSTRACT

We use the observed polarisation properties of a sample of 26 powerful radio galaxies and radio-loud quasars to constrain the conditions in the Faraday screens local to the sources. We adopt the cosmological redshift, low-frequency radio luminosity and physical size of the large-scale radio structures as our ‘fundamental’ parameters. We find no correlation of the radio spectral index with any of the fundamental parameters. The observed rotation measure is also independent of these parameters suggesting that most of the Faraday rotation occurs in the Galactic foreground. The difference between the rotation measures of the two lobes of an individual source as well as the dispersion of the rotation measure show significant correlations with the source redshift, but not with the radio luminosity or source size. This is evidence that the small-scale structure observed in the rotation measure is caused by a Faraday screen local to the sources. The observed asymmetries between the lobes of our sources show no significant trends with each other or other source properties. Finally, we show that the commonly used model for the depolarisation of synchrotron radio emission by foreground Faraday screens is inconsistent with our observations. We apply alternative models to our data and show that they require a strong increase of the dispersion of the rotation measure inside the Faraday screens with cosmological redshift. Correcting our observations with these models for redshift effects, we find a strong correlation of the depolarisation measure with redshift and a significantly weaker correlation with radio luminosity. We did not find any (anti-)correlation of depolarisation measure with source size. All our results are consistent with a decrease in the order of the magnetic field structure of the Faraday screen local to the sources for increasing cosmological redshift.

Key words: Galaxies - active, jets, polarisation, magnetic field

1 INTRODUCTION

The large-scale radio structure of radio galaxies and radio-loud quasars is created by the interaction of powerful jets with the gaseous environment of their host galaxies. The jets themselves are produced in the immediate vicinity of supermassive black holes at the centres of the host galaxies. Because radio radiation is not easily obscured, luminous radio-loud AGN are in principle ideal objects to study the co-evolution of supermassive black holes and their large-scale environments throughout the universe. However, determining the properties of the gas in the surroundings of these objects is not straightforward and a number of techniques have been applied in the past.

Galaxy counts around individual host galaxies can be used to determine the galactic environment, field, group or cluster, of the radio source (e.g. Hill & Lilly, 1991; Wold et al., 2000). Obviously the density of galaxies does not directly yield a constraint on the

properties of the gas in between the galaxies. A relation of galaxy to gas density must be assumed.

The properties of the large-scale radio structure are shaped by the density of the gas the jets are ploughing into. The redshift distribution of, for example, the linear sizes of the lobes of radio galaxies of type FR II (Fanaroff & Riley, 1974) in complete samples can be used to constrain the properties of the source environments (e.g. Kaiser & Alexander, 1999; Blundell et al., 1999). Detailed fitting of two-dimensional radio maps can also be applied to individual sources (Kaiser, 2000). However, the determination of the gas density from the source size is always model-dependent. Although most models for the evolution of radio lobes employ some form or other of ram pressure equilibrium between the jets and the receding gas in the source environment, the model details introduce considerable uncertainty in the estimates of the gas density.

The gas surrounding the lobes of radio galaxies consists of a magnetised plasma which acts as a Faraday screen for the radio synchrotron emission of the lobes. By studying the polarisation properties of the radio emission, we can investigate the properties of this screen. The observable rotation measure caused by the Far-

^{*} email: j.goodlet@talk21.com

day screen depends only on the density of the plasma and also on the strength and orientation of the magnetic field in this material. Despite this degeneracy, we can hope to probe the properties of the gas in the source environments directly. The aim of the present paper is to use this tool to study a sample of 26 powerful radio sources defined in Goodlet et al. (2004, hereafter G04). In order to break the degeneracy due to Malmquist bias between radio-luminosity and redshift observed in previous studies (e.g. Kronberg et al., 1972; Leahy et al., 1986), we defined 3 subsamples of sources chosen from the 3C and 6C/7C catalogues. This selection enables us to investigate any trends of the polarisation properties of our sources with redshift and/or radio luminosity independently.

In Section 2 we briefly describe our sample and the statistical methods we use. We also present the observational data that forms the basis for the subsequent analysis. Section 3 investigates trends of the polarisation properties with ‘fundamental’ source parameters such as redshift, radio luminosity and linear size. Asymmetries between the properties of the two lobes of each source are discussed in Section 4. In Section 5 we show that the polarisation properties of our sources are inconsistent with the commonly used model by Burn (1966) for external Faraday screens. We then apply the more sophisticated models proposed by Tribble (1991) to our data. Finally, Section 6 summarises our main conclusions.

Throughout this paper we use a cosmological model with $H_0 = 75 \text{ km s}^{-1} \text{ Mpc}^{-1}$, $\Omega_m = 0.35$ and $\Omega_\Lambda = 0.65$.

2 DATA AND STATISTICAL METHODS

2.1 Sample description and observables

Our sample of 26 sources is divided into three subsamples. Sample A was defined as a subsample chosen from the 6CE (Eales et al., 1997) subregion of the 6C survey (Hales et al., 1990), and the 7C III subsample (Lacy et al., 1999), drawn from the 7C survey (Pooley et al., 1998). The selected sources have redshifts $0.8 < z < 1.3$, and radio luminosities at 151 MHz of $6.5 \times 10^{26} \text{ W Hz}^{-1} < P_{151\text{MHz}} < 1.35 \times 10^{27} \text{ W Hz}^{-1}$. Sample B was defined as a subsample from the revised 3CRR survey by Laing et al. (1983) containing sources within the same redshift range but with luminosities in the range $6.5 \times 10^{27} \text{ W Hz}^{-1} < P_{151\text{MHz}} < 1.35 \times 10^{28} \text{ W Hz}^{-1}$. Sample C is also from the 3CRR catalogue; it has the same radio luminosity distribution as sample A, but with $0.3 < z < 0.5$. For full details on the sample selection and the data reduction see G04.

In the following we will use source properties derived from the observations: Spectral index, rotation measure and depolarisation. All these properties were averaged over individual lobes. We define the spectral index, α , by $S_\nu \propto \nu^\alpha$. The depolarisation measure, DM , is defined as the ratio of the percentage polarised flux at 4.8 GHz and the percentage polarised flux at 1.4 GHz. The rotation measure, RM , is related to the degree of rotation of the polarisation position angle over a set frequency range, in our case from 1.4 GHz to 4.8 GHz. All source properties used here were determined for individual sources in G04.

The angular resolution of our observations is limited by the need for information on the position angle of the plane of polarisation at 1.4 GHz. For sources with lobes where the degree of polarisation is uniform and the polarisation angle does not change on small scales, we can be confident that our measured depolarisation measures are accurate. However, some sources may exhibit polarisation structure on small angular scales below our resolution limit and for these sources our measurements will be affected by beam

depolarisation. Comparing our maps for the sources at low redshift presented in G04 with the higher resolution maps of Gilbert et al. (2004), obtained mainly at 8 GHz, we find a few sources where beam depolarisation may play a role. Examples include 3C 351 and the northern lobe of 3C 46. Our general impression for this subsample is that sources with distorted lobe structures may suffer from beam depolarisation. This should be borne in mind in the following analysis. Unfortunately, in the absence of better data, particularly for the sources at higher redshifts, it is not possible to quantify this effect.

The difference in the spectral index, depolarisation and rotation measure over the lobes is given by $d\alpha$, dDM and dRM respectively. All differential properties are taken to be the difference of the averages over individual lobes. The rms-variation or dispersion of the rotation measure across a lobe is defined by σ_{RM} .

In G04 we argue that the average rotation measure of the sources, RM , is mainly caused by the interstellar medium in the Galaxy rather than the material in the vicinity of our sources. However, fluctuations in the Faraday screen in the source environment will give rise to the observed variations of RM across the source on smaller spatial scales as measured by dRM and σ_{RM} , as well as the depolarisation, DM . Thus we need to correct for the redshift dependence of these quantities. We correct dRM and σ_{RM} to the sources’ frame of reference by multiplying the measured values by $(1+z)^2$. Note that this factor only corrects for the wavelength dependence of RM . It does not correct for the resolution effects discussed in Section 5. We also adjust DM and dDM to their values appropriate for a uniform cosmological redshift $z = 1$. The latter adjustment requires a model for the structure of the Faraday screen local to the source which gives rise to these measurements. We initially apply the commonly used model presented in Burn (1966, hereafter B66), but discuss alternative, potentially more accurate models that also affect our measurements of σ_{RMz} in Section 5. The adjusted quantities are labelled dRM_z , σ_{RMz} , DM_z and dDM_z . We summarise the observed properties of all sources in our sample in Table 1.

Name	z	$P_{151} / \text{WHz}^{-1}$	ID	D / kpc	$S_{4.8} / \text{mJy}$	α	$RM / \text{rad m}^{-2}$	$\sigma_{\text{RMz}} / \text{rad m}^{-2}$	DM_z
6C 0943+39	1.04	1.0×10^{27}	W	56	31.0	-0.72	1.6	67.0	2.36
			E	45	42.0	-1.01	-19.1	422.0	4.38
6C 1011+36	1.04	1.1×10^{27}	N	175	44.3	-0.88	30.8	53.3	1.60
			S	220	18.7	-0.89	12.6	42.0	1.07
6C 1018+37	0.81	8.8×10^{26}	NE	279	46.4	-0.85	0.85	20.0	1.15
			SW	294	28.7	-0.84	11.2	9.5	1.82
6C 1129+37	1.06	1.1×10^{27}	NW	63	46.5	-0.85	-19.3	229.2	2.86
			SE	69	73.2	-0.90	0.0	93.4	6.35
6C 1256+36	1.07	1.3×10^{27}	NE	69	57.8	-0.79	5.9	93.4	1.42
			SW	62	101.4	-0.87	15.4	60.0	1.01
6C 1257+36	1.00	1.1×10^{27}	NW	134	43.5	-0.71	-115.3	40.0	1.27
			SE	150	20.5	-1.06	-115.6	64.0	1.90
7C 1745+642	1.23	9.5×10^{26}	N	66	23.5	-0.86	—	—	2.71
			S	99	33.8	-0.91	12.8	15.4	1.00
7C 1801+690	1.27	1.0×10^{27}	N	89	8.8	-0.97	44.8	82.5	1.19
			S	113	28.7	-0.81	20.8	51.5	1.73
7C 1813+684	1.03	7.1×10^{26}	NE	282	15.0	-0.92	13.9	350.3	1.02
			SW	152	30.2	-0.79	-68.4	171.8	1.15
3C 65	1.18	1.0×10^{28}	W	83	524.0	-1.00	-82.6	101.7	6.12
			E	68	240.9	-1.03	-86.1	46.1	1.42
3C 68.1	1.24	1.1×10^{28}	N	178	667.2	-0.82	-26.6	139.0	1.45
			S	223	36.8	-1.08	57.9	300.1	2.69
3C 252	1.11	7.2×10^{27}	NW	159	178.7	-1.00	15.7	89.9	1.10
			SE	257	80.0	-1.10	58.5	202.1	2.50
3C 265	0.81	6.5×10^{27}	NW	331	224.0	-0.62	42.2	71.8	1.52
			SE	216	318.9	-0.78	32.8	74.7	1.35
3C 268.1	0.97	1.0×10^{28}	E	151	262.3	-0.92	21.7	41.9	1.52
			W	194	2296.6	-0.58	26.8	51.6	1.82
3C 267	1.14	1.0×10^{28}	E	158	184.0	-1.17	-9.6	111.7	1.43
			W	129	479.2	-0.83	-21.5	107.2	1.08
3C 280	1.00	1.2×10^{28}	E	51	326.0	-1.01	-37.7	80.4	1.83
			W	61	1289.2	-0.76	-7.5	6.0	1.54
3C 324	1.21	1.3×10^{28}	NE	50	432.6	-1.05	22.1	112.3	2.15
			SW	52	166.0	-1.14	43.0	82.0	2.75
4C 16.49	1.29	9.9×10^{27}	N	89	120.0	-0.88	-4.3	295.8	1.10
			S	51	142.3	-1.32	0.9	299.8	1.16
3C 16	0.41	7.4×10^{26}	SW	200	484.9	-0.97	-4.3	34.6	1.16
			NE	187	22.1	-0.87	—	—	1.22
3C 42	0.40	7.5×10^{26}	NW	87	353.9	-0.87	-2.4	27.6	1.01
			SE	92	450.6	-0.86	5.0	27.8	1.00
3C 46	0.44	7.9×10^{27}	NE	512	162.7	-0.94	-4.8	8.1	1.32
			SW	376	173.7	-0.91	-2.9	8.7	1.17
3C 299	0.37	6.9×10^{26}	NE	71	876.5	-0.93	-126.3	142.5	1.15
			SW	36	53.7	-0.71	16.0	12.9	1.04
3C 341	0.45	8.8×10^{26}	NE	280	123.8	-0.85	20.3	21.0	1.11
			SW	145	265.9	-1.00	18.2	25.2	1.13
3C 351	0.37	7.6×10^{26}	NE	158	1093.9	-0.80	1.0	23.5	1.02
			SW	188	77.1	-0.93	4.4	20.3	1.24
3C 457	0.43	9.6×10^{27}	NE	568	208.6	-1.02	—	—	1.00
			SW	519	290.5	-0.94	—	—	1.05
4C 14.27	0.39	8.8×10^{26}	NW	103	107.0	-1.06	-13.0	10.4	1.09
			SE	76	124.8	-1.17	-17.3	9.3	1.01

Table 1. Observational properties of the sources in our sample. P_{151} is the radio luminosity at 151 MHz, D the physical size of individual lobes and $S_{4.8}$ is the radio flux at 4.8 GHz. σ_{RMz} is the dispersion of the rotation measure corrected for redshift effects. DM_z is the depolarisation adjusted to a common redshift of $z = 1$ using the model of Burn (1966). All data taken from G04.

2.2 Statistical methods

In this paper we use the Spearman Rank test (SR), the Partial Spearman Rank test (PSR) and Principal Component Analysis (PCA). SR is a non-parametric correlation test which assigns a rank to given source properties, say X and Y , and computes the coefficient of the correlation, r_{XY} , between the ranks. By definition $-1 \leq r_{XY} \leq 1$, where negative values of r_{XY} indicate an anti-correlation. The null hypothesis that no correlation is present corresponds to $r_{XY} = 0$ and in general r_{XY} has a Student-t distribution. A (anti-)correlation with a confidence level exceeding 95% will result in a Student-t value greater than 2 for the size of our sample (e.g. Riley et al., 1997).

PSR tests whether a correlation between properties X and Y is due to independent individual correlations of X and Y with a third property Z (e.g. Macklin, 1982). The correlation coefficient, $r_{XY,Z}$, increases (decreases) from zero if the correlation (anti-correlation) is predominantly between X and Y , independent of Z . The positive significance of the (anti-)correlation is measured by $D_{XY,Z}$.

PCA is a multi-variate statistical test (e.g. Deeming, 1964; Efsthathiou & Fall, 1984). PCA is a linear self-orthogonal transformation from an original set of n objects and m attributes forming a $n \times m$ matrix, with zero mean and unit variance, to a new set of parameters, known as principal components. The principal components of the new dataset are all independent of each other and hence orthogonal. The first component describes the largest variation in the data and has, by definition, the largest eigenvalue of the $n \times m$ matrix. In physical terms the magnitude of the eigenvalue determines what fraction of the variance in the data any correlation describes. Thus a strong correlation will be present in the first eigenvector and will only strongly reverse in the last. PCA in its simplest terms is an eigenvector-eigenvalue problem on a transformed, diagonalised and standardised set of variables. n objects will create an eigenvector-eigenvalue problem in $n - 1$ dimensions. To avoid problems with the interpretation of our results, we do not use more than 4 parameters in any part of the analysis.

3 TRENDS WITH REDSHIFT, LUMINOSITY AND SIZE

The aim of our analysis is to investigate any trends with redshift and/or radio luminosity of observables that may depend on the properties of the gas surrounding the radio lobes of our sample sources. Another important parameter that may influence our results is the physical size of the radio lobes. Because we expect significant gradients for the gas density in the typical environments of sources, the properties of small sources will clearly be shaped by very different conditions than those of large sources, even if the overall gaseous environment is the same. Many studies have investigated the dependence of the average size of sources as a function of redshift and radio luminosity in complete samples of sources (e.g. Singal, 1988; Barthel & Miley, 1988; Kapahi, 1989; Singal, 1993; Neeser et al., 1995; Kaiser & Alexander, 1999; Blundell et al., 1999). This is not the purpose of the study presented here. Our sample is not complete and sources were selected in order to cover an equal range of physical sizes within our sample limits of redshifts and radio luminosities.

In the following we will refer to the redshift, z , radio luminosity at 151 MHz, P , and the physical size, D , as the ‘fundamental’ source parameters. In order to better understand the correlations of other observables with the fundamental parameters, we first need to investigate any correlations between them. This analysis also serves as a useful test of the robustness of our sample selection.

X, Y	r_{XY}	Student-t	Z	$r_{XY,Z}$	$D_{XY,Z}$
z, P	0.70	4.8	D	0.69	4.0
z, D	-0.23	-1.2	P	0.04	0.20
P, D	-0.13	-0.64	z	-0.20	0.93

Table 2. Spearman Rank coefficients for correlations between the fundamental parameters.

X, Y	r_{XY}	Student-t	X, Y	r_{XY}	Student-t
α, z	-0.13	-0.62	$d\alpha, z$	0.15	0.77
α, P	0.04	0.19	$d\alpha, P$	0.27	1.35
α, D	0.21	1.05	$d\alpha, D$	-0.21	-1.05

Table 3. Spearman Rank coefficients for the correlations between spectral index, α , and difference of spectral index between lobes, $d\alpha$, and the fundamental parameters.

Table 2 illustrates the relations between the fundamental parameters in our sample. Clearly, redshift and radio luminosity are strongly correlated, but this correlation simply follows from our sample selection. Using the statistical techniques described above, we can isolate this correlation from others. In fact, it provides us with a ‘bench mark’ for other correlations.

The SR results also imply a weak anti-correlation between the redshift of a source and its physical size. However, the PSR results show that the relation between the three fundamental parameters is more complex than a simple anti-correlation between z and D . We also found that the anti-correlation disappears if the two exceptionally large sources 3C 46 and 3C 457, both at low redshifts, are removed from the sample. In practice, the z - D anti-correlation is too weak to introduce any significant bias into our results. We therefore conclude that our sample contains a sufficient range of physical sizes at each redshift and radio luminosity.

In the following we investigate not only the observed source properties, but also differences of these properties between the two lobes of each source. Clearly there are twice as many direct measurements of, say, the spectral index of individual lobes, than measurements of the difference of the spectral index between the lobes. To avoid complications with the different number of measurements, we always use values for all source properties averaged over the entire source.

3.1 Spectral index

The dependence of the spectral index, α , on the fundamental parameters for radio galaxies of type FR II has been investigated by various authors. Véron et al. (1972) and Onuora (1989) find a strong spectral index–radio luminosity correlation, but no corresponding correlation with redshift. Interestingly Athreya & Kapahi (1999) find a strong correlation of spectral index with redshift, but no significant correlation with radio luminosity. Finally, Blundell et al. (1999) find that α is anti-correlated not only with radio-luminosity, but also with source size. They found that in general, larger sources had a steeper spectral index.

In our sample there is no clear trend of the spectral index with any of the fundamental parameters (Tables 3 and 4). The difference in the spectral index of the lobes, $d\alpha$, also shows no significant correlations with the fundamental parameters. The absence of the

	Eigenvector			
	1	2	3	4
z	0.64	-0.25	0.06	-0.73
P	0.58	-0.16	0.53	0.60
D	-0.47	-0.12	0.82	-0.31
α	-0.21	-0.95	-0.21	0.13
Variation	45%	25%	21%	10%
z	0.56	-0.08	0.54	-0.62
P	0.55	0.44	0.26	0.66
D	-0.40	0.84	0.19	-0.30
$d\alpha$	0.48	0.30	-0.77	-0.29
Variation	51%	21%	18%	10%

Table 4. PCA results for the spectral index and the fundamental parameters.

X, Y	r_{XY}	Student-t	X, Y	r_{XY}	Student-t
RM, z	0.17	0.79	dRM, z	0.50	2.65
RM, P	0.27	1.31	dRM, P	0.23	1.06
RM, D	-0.05	-0.23	dRM, D	-0.22	-1.05
σ_{RMz}, z	0.68	4.24			
σ_{RMz}, P	0.35	1.71			
σ_{RMz}, D	-0.30	-1.46			

Table 5. Spearman Rank coefficients for the correlations between rotation measure, RM , the difference of the rotation measure between lobes, dRM , and the dispersion of the rotation measure, σ_{RMz} , and the fundamental parameters.

trends claimed in the literature from our sample is probably due to the small sample size.

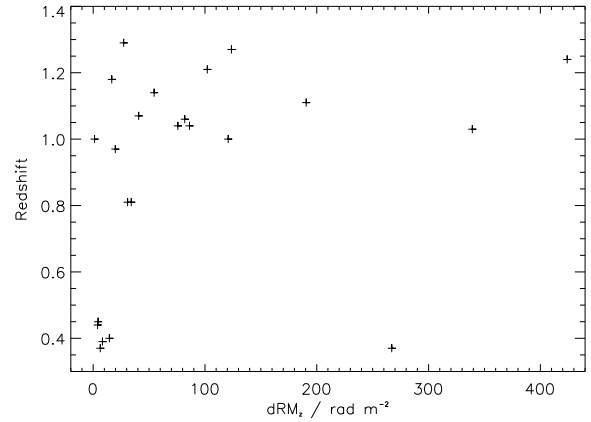
3.2 Rotation measure

The SR results in Table 5 show that there are no strong correlations of the fundamental parameters with rotation measure, RM . In every case the correlation is below 95% significant. The PCA results in Table 6 also demonstrate that the RM of a source does not depend on the size, redshift or the radio luminosity of the source. This is consistent with our interpretation that the observed RM is caused by the Galactic magnetic field and not by Faraday screens local to the sources (G04; Leahy 1987).

The difference in the rotation measure, dRM_z , between the two lobes of a given source and the dispersion of the rotation measure, σ_{RMz} , are probably caused locally to the source and have therefore been corrected to the sources' frame of reference (G04). There is a dRM_z - z correlation present in the SR results, (see Table 5), but it is weaker in the PCA results where the correlation is strongly reversed in the 3rd eigenvector (see Table 6). Figure 1 shows that in principal we should find a strong dRM_z - z correlation. However, the presence of the source 3C 299 at low redshift, but with a large value of dRM_z weakens this trend. The large value of dRM_z for 3C 299 is due to a lack of polarisation information in one lobe. Removing this source strengthens the correlation giving $r_{dRM_z, z} = 0.632$ which corresponds to a significance of 99.98%.

σ_{RMz} measures variations of the Faraday screen on scales smaller than dRM_z , which may in principle be influenced by the Galactic Faraday screen. However, it is interesting to note that dRM_z correlates strongly with σ_{RMz} (see Figure 2). So the two pa-

	Eigenvector			
	1	2	3	4
z	0.64	0.24	-0.05	-0.73
P	0.60	0.41	-0.17	-0.67
D	-0.38	0.44	-0.80	0.13
RM	0.30	-0.76	-0.57	-0.05
Variation	44%	24%	22%	11%
z	0.63	-0.02	0.22	0.74
P	0.58	-0.12	0.49	-0.64
D	-0.32	-0.86	0.36	0.14
dRM_z	0.40	-0.49	-0.76	-0.13
Variation	46%	23%	20%	11%
z	0.62	0.18	0.06	0.76
P	0.49	0.42	-0.62	-0.45
D	-0.32	0.89	0.33	0.03
σ_{RMz}	0.52	-0.06	0.71	-0.47
Variation	51%	22%	19%	8%

Table 6. PCA results for the rotation measure and the fundamental parameters.**Figure 1.** Redshift against difference in rotation measure, dRM_z across the lobes of a source. dRM_z has been shifted to the sources' frame of reference.

rameters may sample the same, local Faraday screen even if dRM_z may still contain some Galactic contribution.

σ_{RMz} shows a strong correlation with redshift, $> 99.9\%$ significance, and a weak anti-correlation with D . The σ_{RMz} - z correlation also strengthens with the removal of 3C 299, becoming $r_{\sigma_{RMz}, z} = 0.767$ which corresponds to a significance exceeding 99.99%. These correlations are more obvious when the PCA results are considered (see Table 6). The first eigenvector contains 51% of the variation in the data and shows a strong z - σ_{RMz} correlation and a weaker D - σ_{RMz} anti-correlation. The D - σ_{RMz} anti-correlation reverses in the third eigenvector indicating that it is a considerably weaker trend compared to the z - σ_{RM} correlation which only reverses in the last eigenvector. The PSR results in Table 7 confirm that there are no significant correlations with radio luminosity for both dRM_z and σ_{RMz} .

In a survey of 27 high redshift sources Pentericci et al. (2000) found that the Faraday rotation was independent of size or ra-

6 Goodlet & Kaiser

X,Y	Z	$r_{XY,Z}$	$D_{XY,Z}$
z, dRM_z	P	0.49	2.40
z, P	dRM_z	0.69	3.79
P, dRM_z	z	-0.19	0.86
z, σ_{RMz}	P	0.65	3.47
z, P	σ_{RMz}	0.67	3.63
P, σ_{RMz}	z	-0.24	1.09

Table 7. PSR coefficients for correlations of dRM_z and σ_{RMz} with the fundamental parameters.

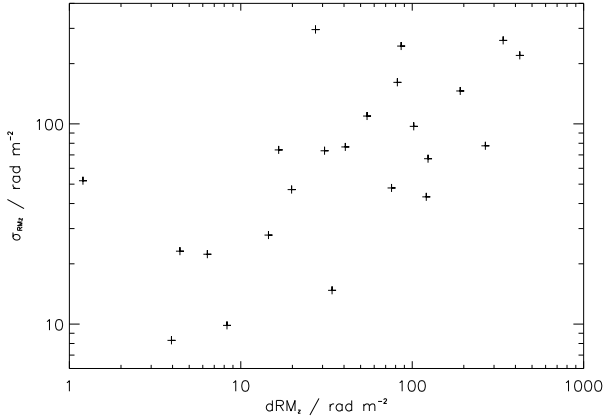


Figure 2. The dispersion of the rotation measure, σ_{RMz} , against the difference in rotation measure across the lobes of a source, dRM_z .

dio luminosity, but also showed that the number of sources with high levels of Faraday rotation increased with redshift. The results from Pentericci et al. (2000) use the RM of a source in the sources' frame of reference. As noted in G04 and above, the RM observed in our sources is dominated by contributions from the Galaxy. Therefore we cannot directly compare our results with those of Pentericci et al. (2000). Also note that the sample of Pentericci et al. (2000) contains only sources at considerably higher redshifts than our sample.

The trend reported in Pentericci et al. (2000) indicates that the strength of the magnetic field and/or the density of the environment is increasing with redshift. Which effect dominates cannot be decided from RM measurements alone. Similarly, we use σ_{RMz} and dRM_z which also do not provide us with a direct measurement of the density or the strength of the magnetic field in the vicinity of our sources. However, our indicators depend strongly on the degree of order in the direction of the magnetic field in the local Faraday screen. Thus our results point towards a trend for more chaotic magnetic field structures in the source environments at higher redshift.

3.3 Depolarisation

Depolarisation arises from structure of the magnetic field in the Faraday screen at scales below the telescope resolution. In the previous Section we already found that the measured dispersion of RM is correlated with the redshift of the source, indicating that the small-scale structure in the RM arises from a Faraday screen local to our sources. Therefore we expect that the depolarisation also correlates with redshift in our sample. Clearly we must also correct

X, Y	r_{XY}	Student-t	X, Y	r_{XY}	Student-t
DM_z, z	0.69	4.66	dDM_z, z	0.74	5.39
DM_z, P	0.69	4.65	dDM_z, P	0.54	3.18
DM_z, D	-0.31	-1.61	dDM_z, D	-0.31	-1.60

Table 8. Spearman Rank coefficients for the correlations between depolarisation, DM_z and the difference of the depolarisation between lobes, dDM_z , and the fundamental parameters.

	Eigenvector			
	1	2	3	4
z	0.58	0.22	0.0	-0.78
P	0.47	0.67	-0.19	0.54
D	-0.44	0.61	0.64	-0.16
DM_z	0.50	-0.35	0.75	0.27
Variation	53%	22%	16%	10%
z	0.60	0.19	0.01	0.78
P	0.48	0.68	-0.22	-0.52
D	-0.43	0.63	0.62	0.17
dDM_z	0.49	-0.33	0.75	-0.30
Variation	52%	22%	17%	10%

Table 9. PCA results for the depolarisation and the fundamental parameters.

X,Y	Z	$r_{XY,Z}$	$D_{XY,Z}$
z, DM_z	P	0.40	2.00
z, P	DM_z	0.44	2.21
P, DM_z	z	0.41	2.04
z, dDM_z	P	0.60	3.25
z, P	dDM_z	0.53	2.77
P, dDM_z	z	0.05	0.23

Table 10. PSR coefficients for correlations of DM_z and dDM_z with the fundamental parameters.

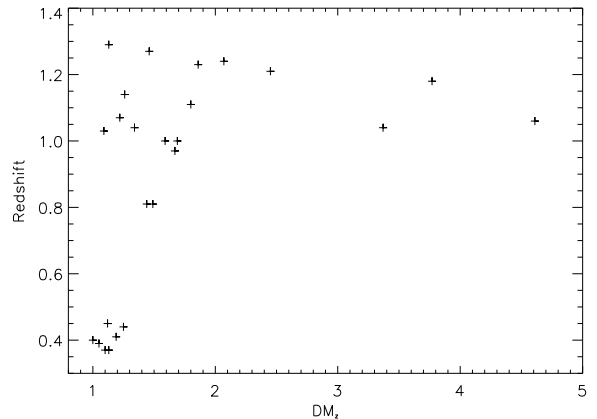


Figure 3. Redshift against the average depolarisation of a source. The depolarisation has been shifted to a common redshift, $z = 1$.

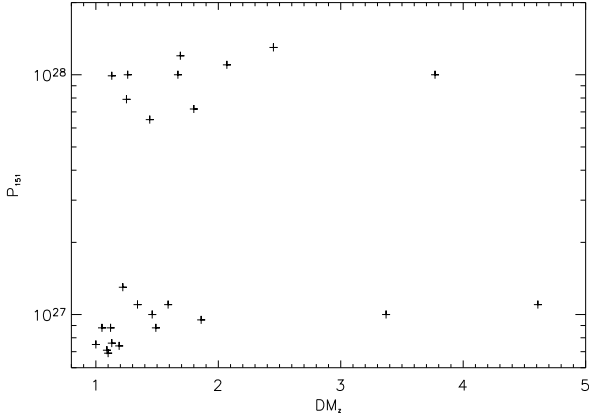


Figure 4. Radio-luminosity against the average depolarisation. The depolarisation has been shifted to a common redshift, $z = 1$.

our measured DM values for redshift effects. In this Section we apply the commonly used model of B66 to adjust DM and dDM to a common redshift of $z = 1$ for all our sources to allow for a direct comparison. In Section 5 we will investigate alternative models.

There is little difference between the redshift and the radio luminosity correlations with the average adjusted depolarisation, taken over the source as a whole, DM_z , (see Table 8) as both correlations show significance levels in excess of 99.9%. There is also an indication of a DM_z - D anti-correlation, but this trend is not significant. We use the Partial Spearman Rank test to determine if the P - DM_z correlation can be explained by the independent z - DM_z and z - P correlations (see Table 10). Again we find little difference between the redshift and radio-luminosity correlations. This result is also confirmed by the PCA results in Table 9. Figure 3 shows that the higher redshift sources display, on average, a larger degree of depolarisation and also a much larger spread of depolarisation at any given redshift compared to their low redshift counterparts. There is little difference in the range of DM_z between sources with very different radio luminosity (see Figure 4). However, this result may be caused by only two sources of low radio luminosity and exceptionally high values of DM_z . Previous studies of the correlation of depolarisation with redshift and/or radio luminosity are also inconclusive. Morris & Tabara (1973) found depolarisation to correlate with radio luminosity whereas Kronberg et al. (1972) found the correlation was predominantly with redshift. In view of the stronger correlation of σ_{RMz} with redshift it is surprising that DM_z does not show a correlation with redshift that is significantly stronger than the correlation with radio luminosity. However, we show in Section 5 that this result depends on which model for the local Faraday screen is used to correct for redshift effects.

The difference in the depolarisation over the source, dDM_z , shows a stronger trend with redshift than the overall depolarisation, DM_z (Tables 8 and 9). The PSR results, Table 10, indicate a significant correlation between redshift and dDM_z at any given radio luminosity. The corresponding P - dDM_z correlation is considerably weaker at a given redshift.

Table 8 shows a weak DM_z - D anti-correlation. The PCA results in Table 9 confirm that this result is not very significant. However, a DM_z - D anti-correlation has been reported by Strom (1973); Strom & Jägers (1988); Pedelty et al. (1989, hereafter P89), Best et al. (1999) and Ishwara-Chandra et al. (1998), but was not found by Dennett-Thorpe (1996). The observations by

Strom (1973), Strom & Jägers (1988) and Ishwara-Chandra et al. (1998) are at a lower resolution than our measurements and thus their different findings may be due to this resolution difference. The observations by Best et al. (1999) are at a higher resolution, but also at higher frequencies (4.8 GHz to 8.4 GHz) and so we would expect any depolarisation trends to be stronger in this sample. Both P89 and Dennett-Thorpe (1996) however observe the same frequency range and with the same spatial resolution as in our sample. Even when our results from sample B, which are taken at the most similar redshift and radio-luminosity range to those of P89, are analysed separately, we still find no trend with size. There is no obvious difference in the selection of the P89 sample and our sample B, except that P89 chose their sample from sources which had strong emission lines. By preferentially selecting sources with strong emission lines P89 have chosen sources with jet axes close to our line of sight. This selection may strengthen any D - DM correlation found. However, we do not have a convincing physical explanation why our results differ from the ones of P89 because of this selection criterion.

It is usually assumed that radio sources are located in stratified atmospheres. Therefore a small source will be embedded in denser gas which acts as a more efficient Faraday screen. As the source expands the lobes will extend beyond the denser inner atmosphere, thus reducing the amount of depolarisation observed. In the beginning of Section 3 we showed that there is no significant z - D anti-correlation in our sample. Therefore the lack of a pronounced DM_z - D anti-correlation suggests that there is no significant difference in the source environments at any redshift as the sources become larger. This may be evidence that the environments of our sources are relatively homogeneous with little stratification. The lack of an anti-correlation between the source size, D , and dDM_z (see Tables 8 and 9) is consistent with this idea.

4 SOURCE ASYMMETRIES

In Section 3 we investigated the trends of observables averaged over the entire structure of our sources with respect to redshift, total low-frequency radio luminosity and overall source size. In this Section we study in detail the asymmetries between the lobes of our sources, in particular how differences in the lengths and radio fluxes of lobes of individual sources relate to asymmetries in other observable properties. In the following discussion on possible mechanisms that could give rise to asymmetries between the two lobes of a source, we assume that the two jets of a given source are not significantly different from each other in terms of their energy transport rate.

The angle at which a source is orientated to the line-of-sight affects the projected lobe length. Because of finite light travel times sources orientated at a small angle will have lobes that appear more asymmetrical than sources at a large angle, assuming there are no differences between the environments of the two lobes. Assuming a source is orientated at an angle θ to the line-of-sight, then the ratio of lobe lengths, D_1/D_2 , is given by (e.g. Longair & Riley, 1979)

$$\frac{D_1}{D_2} = \frac{1 + (v_o/c) \cos\theta}{1 - (v_o/c) \cos\theta}, \quad (1)$$

where v_o is the velocity at which the hotspot is moving away from the nucleus and c is the speed of light. The orientation of a source will also induce asymmetries in the the rotation measure and the depolarisation (e.g. Garrington & Conway, 1991). In a simple orientation model emission from the lobe pointing away from the

observer will have a longer path length through the local Faraday screen and thus any depolarisation measurements of this lobe would be larger than the lobe pointing towards the observer, which is referred to as the Laing-Garrington effect.

The motion of material in the radio hotspots at the end of the lobes of FR II-type sources is likely to be relativistic. Relativistic beaming can therefore also cause asymmetries in a source, independent of path length through the Faraday screen. As the hotspot becomes increasingly more beamed, i.e. $\theta \rightarrow 0$, the lobe ratio increases. The flat radio spectrum of the hotspot will begin to dominate the flux and spectral index in the beamed lobe. Thus as relativistic beaming becomes more dominant in a source, the beamed lobe will become brighter, longer and its spectrum flatter than the receding lobe. Liu & Pooley (1991a) also find for sources in their sample that the least depolarised lobe has a flatter spectrum.

Finally, differences in the environments of the two lobes may also introduce asymmetries. For example, theoretical models for the evolution of radio lobes predict that denser environments lead to shorter and brighter lobes with steeper spectral indices (e.g. Kaiser et al., 1997). A jet with a given energy transport rate will expand more slowly in a dense environment compared to the situation in less dense surroundings. The pressure in the lobe as well as the strength of the magnetic field will be higher. The increased strength of the magnetic field will lead to increased energy losses of the radiating relativistic electrons, resulting in a steeper spectral index. Thus a source situated in an environment with an asymmetrical density distribution will develop asymmetrical lobes. In the following we will use the lobe asymmetries observed in our sample in an attempt to distinguish between these possibilities.

In Section 3 we only used the overall physical size of our sources, D . We now need to measure the lengths of individual lobes. In about half of our sources we do not detect a radio core at our two observing frequencies. In these cases, wherever possible, we used previously published maps to establish the core position. However, in several sources, most notably 3C 16, no core is reported in the literature. We estimated the location of the core position by using the most likely core position from the literature (Liu & Pooley, 1991b). This approach is not ideal, but as our maps are not of very high resolution, the values calculated for the lobe length will only be approximations to the true lengths in any case.

In Section 3 we adjusted the measured depolarisation to a common redshift of $z = 1$. For this correction we had to assume a specific underlying structure of the Faraday screen. Here we compare the two lobes of a given source and so we can use the uncorrected depolarisation to avoid any model dependence. This choice is consistent with previous studies (P89; Liu & Pooley 1991a; Garrington & Conway 1991) which also used the observed, uncorrected depolarisation.

4.1 Lobe length and radio flux

Figure 5 shows the ratio of lobe lengths as a function of overall physical size of the sources. Most of our sources are quite symmetric and there is no tendency for smaller sources to show larger lobe length asymmetries than larger sources.

We use the radio flux at 4.8 GHz in our study of the source asymmetries, since it has lower noise levels than the 1.4 GHz data (G04). Figure 6 demonstrates that for all sources the flux of the brighter lobe is tightly correlated with the flux of the fainter lobe. In a few cases the flux of the fainter lobe is much smaller than the flux of the brighter lobe. Three of these very asymmetrical sources are quasars, 3C 351, 3C 68.1 and 3C 16, the jet axes of which are pre-

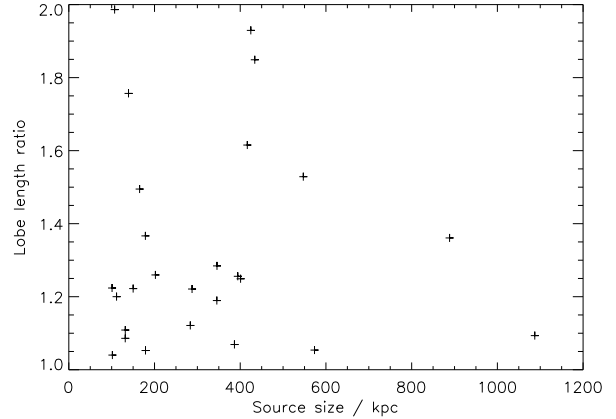


Figure 5. Plot of the lobe ratio against the physical size of the entire radio structure of our sources.

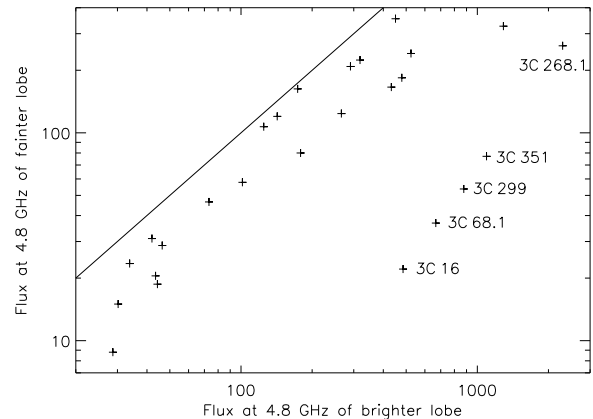


Figure 6. Plot of the flux of the fainter lobe against the brighter lobe at 4.8 GHz. The line shows the location of sources for which the luminosities of the two lobes are identical.

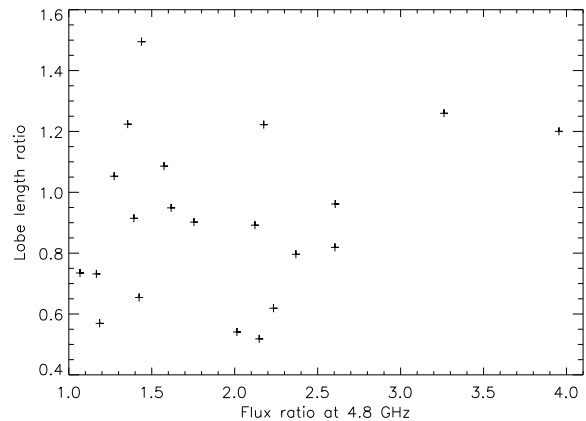


Figure 7. Plot of the lobe ratio against the flux ratio at 4.8 GHz, omitting the sources with an exceptional flux asymmetry, 3C 299, 3C 268.1, 3C 16, 3C 351 and 3C 68.1.

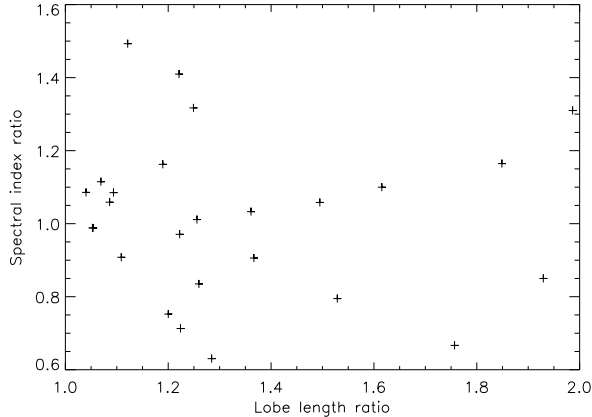


Figure 8. Plot of the spectral index ratio against the lobe ratio.

sumably closely aligned with our line of sight probably leading to the large flux asymmetry. The radio galaxies 3C 299 and 3C 268.1 also show a large flux asymmetry. The pronounced asymmetry of 3C 299 was also noted by McCarthy et al. (1995), who suggest that despite its low redshift the source shows characteristics of a high redshift ($z > 1$) radio galaxy. We also find 3C 299 to have a σ_{RM} comparable to the high redshift samples.

Harvanek & Stocke (2002) noted that 3C 299 has lobes of very different lengths. In fact, it is the source with the largest length asymmetry in our sample. The other four sources showing a large flux asymmetry do not have unusual lobe ratios. However, it should be noted that the cores in 3C 68.1 and 3C 16 have not been detected in our observations or previously. Bridle et al. (1994) do marginally detect a core in deeper observations of 3C 68.1 and we have used their core position in determining the lobe lengths of this source. To further aggravate the problem, both, 3C 16 and 3C 68.1, have very faint lobes and so it is hard to determine where exactly the lobe terminates. However, it is worth noting that when the 5 unusual sources are removed from consideration there is no significant trend for the sources with a large flux ratio to also show strong length asymmetries (see Figure 7). This argues against the interpretation that the source asymmetries are caused by differences in the gaseous environments of the two lobes of a source.

We do not find any trends of the flux asymmetries with either redshift or radio luminosity.

4.2 Spectral index

The spectral index ratio shows no correlation with the lobe length ratio (see Figure 8). If differences in the gaseous environment of the lobes were the source of the observed asymmetries, then we would expect that the lobe located in the denser environment is shorter and has a steeper radio spectrum (e.g. Kaiser et al., 1997). This result therefore argues against different lobe environments. However, it is consistent with relativistic beaming of the flat-spectrum hotspot emission, if the lobe length asymmetry is due to only small differences in the gas density of their environments.

Neglecting the five sources with unusually large flux asymmetries, we find that in sources with a large flux asymmetry the brighter lobe has a flatter spectral index than the fainter lobe (see Figure 9). For more symmetric sources the range of the spectral index ratio is larger with a weak tendency for the brighter lobe to have a steeper spectral index than the fainter lobe. Both results are

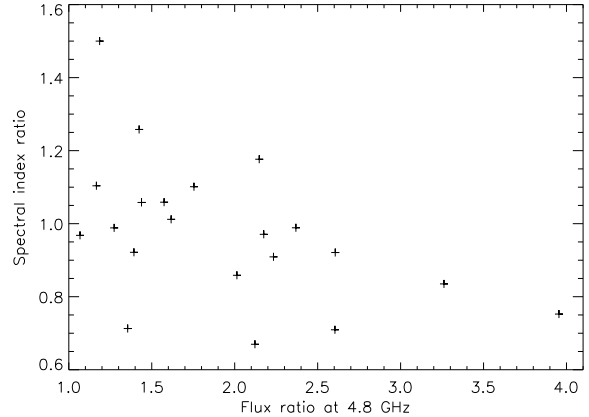


Figure 9. Plot of the spectral index ratio against the flux ratio at 4.8 GHz, omitting the sources with an exceptional flux asymmetry, 3C 299, 3C 268.1, 3C 16, 3C 351 and 3C 68.1.

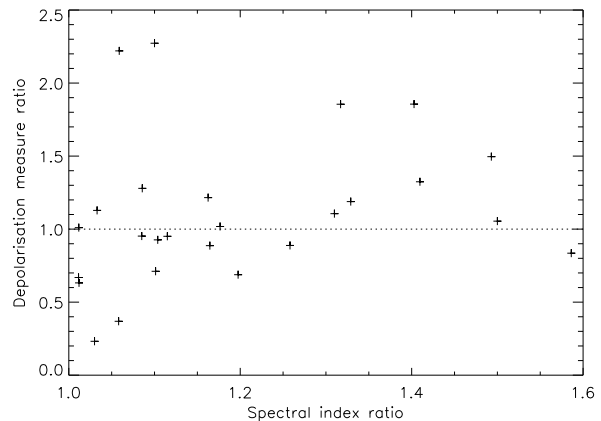


Figure 10. Plot of the depolarisation measure ratio against the spectral index ratio. Sources above the dotted line follow the trend proposed by Liu & Pooley (1991a).

again consistent with asymmetries arising from relativistic beaming of the hotspot emission. Lobes for which beaming is more important will be dominated by their bright hotspots which have a flat radio spectrum. Relativistic beaming is less important for sources oriented close to the plane of the sky. For these objects small differences in the density of the lobe environments may lead to a brighter lobe with a steeper spectrum located in the denser surroundings.

Liu & Pooley (1991a) study a sample of 13 sources, for 12 of which the lobe with the steeper spectrum is also the most depolarised lobe. Figure 10 illustrates that only 14 of our 26 sources are consistent with this trend. However, our findings are consistent with those of Ishwara-Chandra et al. (2001) who also find only 58% of radio galaxies and 59% of quasars in their much larger sample to agree with the result of Liu & Pooley (1991a). The distribution in Figure 10 suggests that sources with a larger spectral index asymmetry are more likely to follow the proposed trend. Again this is consistent with the asymmetries arising from relativistic beaming of the hotspot emission. In this scenario, the lobe with the steeper spectral index points preferentially away from the observer. The radio emission from this lobe has to traverse a longer path through

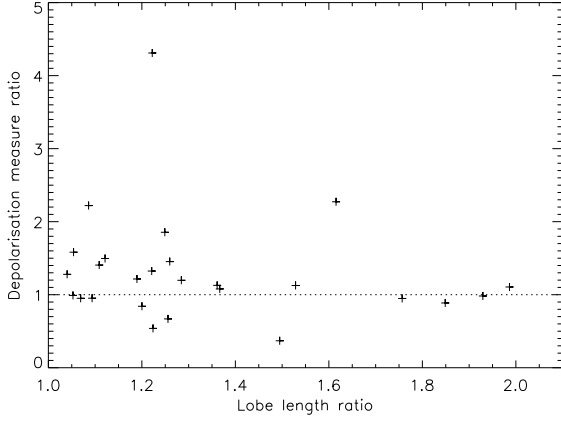


Figure 11. Plot of the depolarisation measure ratio against the lobe length ratio. For sources above the dotted line the larger lobe is also more depolarised.

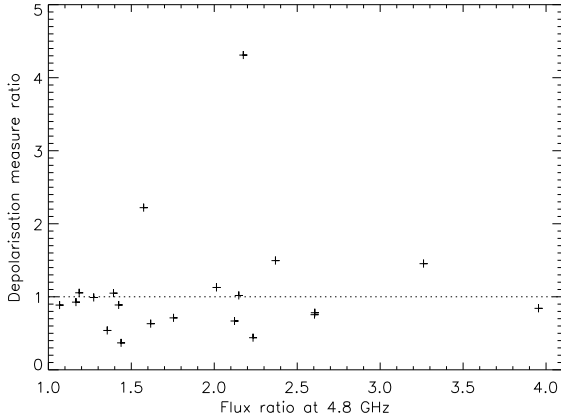


Figure 12. Plot of the depolarisation measure ratio against the flux ratio at 4.8 GHz, omitting the sources with an exceptional flux asymmetry, 3C 299, 3C 268.1, 3C 16, 3C 351 and 3C 68.1. For sources above the dotted line the brighter lobe is also more depolarised.

the surrounding medium which acts as a Faraday screen, leading to greater depolarisation.

4.3 Depolarisation

In Figure 11 we compare the depolarisation measure ratio with the ratio of the lobe lengths. For 16 of our 26 sources the larger lobe is also more depolarised. Our result disagrees with the findings of P89 and Liu & Pooley (1991a), but is consistent with Dennett-Thorpe (1996). The cause for this difference may be the different sample selection criteria, but the trend is not very strong in any of the studies considered here.

The same is true for the relation between the depolarisation measure ratio and the flux ratio (see Figure 12). Neglecting the five sources with large flux ratios, for 13 of the remaining 21 sources the brighter lobe is less depolarised. Although this is consistent with the beaming scenario, the trend is not very significant.

In summary the trends we find in our sample favour relativistic beaming of the hotspots as the underlying mechanism giving rise

to the observed source asymmetries. However, none of the trends is very significant and so our results should be treated with caution.

5 DEPOLARISATION BEYOND BURN'S LAW

Depolarisation of radio synchrotron emission by a Faraday screen external to the radiation source arises from the inhomogeneity of the magnetic field in the screen combined with limited spatial resolution of the observations. Let the magnetic field and gas density in the Faraday screen be coherent in ‘cells’ of a typical size s_0 . The physical size of the telescope beam at the position of the source is t . For $t \ll s_0$ we resolve the Faraday screen and no depolarisation takes place. In fact, by mapping the rotation measure, we are mapping the structure of the Faraday screen in this case. However, usually t is comparable to or larger than s_0 and so one beam contains several cells with different position angles of the polarisation vector, \mathbf{p} . The average polarisation, $\langle |\mathbf{p}| \rangle \equiv p$, is therefore reduced by the partial cancellation of polarisation vectors associated with individual cells within the beam. Clearly, the physical size of the telescope beam depends on the redshift of a source and so p depends in general on z even if the structure of the Faraday screen does not change as a function of redshift.

In previous sections we have used Burn’s law (B66) to correct our measured depolarisation for redshift effects. However, this model of the external Faraday screen only applies if the structure of the Faraday screen is Gaussian and, more importantly, if $s_0 \ll t$, i.e. for cases where the structure of the Faraday screen is completely unresolved. For Cygnus A Carilli & Barthel (1996) report coherent RM fluctuations on scales of $s_0 \sim 10$ kpc from observations resolving individual cells. At least in this source we have $s_0 \sim t$ and Burn’s law does not apply.

5.1 Alternatives to Burn’s law

If we cannot assume that $s_0 \ll t$, we need to take into account the autocorrelation or structure function of the rotation measure cells in the external Faraday screen to derive estimates for the observed RM and polarisation properties of our sources. We follow the approach by Tribble (1991, hereafter T91), assuming a Gaussian random RM field with dispersion σ and three different structure functions, $D(s)$, where s measures physical distance projected on the plane of the sky. Also, because of the limit set by the resolution of our observations at wavelength λ , the RM dispersion we measure, σ_{RMz} , is not equal to the underlying, ‘true’ dispersion, σ . In detail we have:

- Quadratic structure function with

$$\begin{aligned} D(s) &= 2\sigma^2 (s/s_0)^2, \text{ for } s < s_0 \\ D(s) &= 2\sigma^2, \text{ for } s \geq s_0, \end{aligned} \quad (2)$$

leading to

$$\begin{aligned} \langle |\mathbf{p}|^2 \rangle &= \frac{1 - \exp(-\beta - \gamma)}{1 + \gamma/\beta} + \exp(-\beta - \gamma), \\ \sigma_{RMz}^2 &= \sigma^2 \{1 - [1 - \exp(-\beta)]/\beta\}. \end{aligned} \quad (3)$$

- Gaussian autocorrelation function with

$$D(s) = 2\sigma^2 \left[1 - \exp\left(-s^2/s_0^2\right)\right], \quad (4)$$

leading to

$$\langle |\mathbf{p}|^2 \rangle = \beta \exp(-\gamma) \int_0^1 x^{\beta-1} \exp(\gamma x) dx,$$

		σ / rad m ⁻²	s_0 / kpc
Varying s_0	Quadratic	530	$0.15(1+z)^{4.1}$
	Gaussian	500	$0.11(1+z)^{4.2}$
	Power-law, $m = 2$	490	$0.03(1+z)^{5.1}$
	Power-law, $m = 4$	460	$0.08(1+z)^{4.4}$
Varying σ	Quadratic	$5.0(1+z)^{4.9}$	10.
	Gaussian	$5.1(1+z)^{4.7}$	10.
	Power-law, $m = 2$	$5.1(1+z)^{4.5}$	10.
	Power-law, $m = 4$	$5.1(1+z)^{4.6}$	10.

Table 11. Summary of best-fitting model parameters for the dispersion of the rotation measure, σ_{RM} .

$$\sigma_{\text{RMz}}^2 = \frac{\sigma^2}{1 + 1/\beta}. \quad (5)$$

- Power-law autocorrelation function with

$$D(s) = 2\sigma^2 \left[1 - \left(1 + 2s^2/ms_0^2 \right)^{-m/2} \right], \quad (6)$$

leading to

$$\begin{aligned} \langle |\mathbf{p}|^2 \rangle &= \frac{m}{2} \beta \exp(\beta - \gamma), \\ &\int_1^\infty \exp(-m\beta x/2) \exp(\gamma x^{-m/2}) dx \\ \sigma_{\text{RMz}}^2 &= \sigma^2 (m\beta/2)^{m/2} \Gamma(1 - m/2, m\beta/2) \exp(m\beta/2). \end{aligned} \quad (7)$$

Here we used the definitions $\beta = s_0^2/2t^2$, $\gamma = 4\sigma^2\lambda^4$ and

$$\Gamma(a, x) = \int_x^\infty \exp(-t) t^{a-1} dt \quad (8)$$

for the incomplete Γ -function. The polarised flux can be obtained from $p^2 = \langle |\mathbf{p}|^2 \rangle$ for a Gaussian telescope beam.

The physical size of the telescope beam at the source location, t , is given by the resolution of the telescope and the adopted cosmological model. The quadratic and Gaussian structure functions then have two free parameters, the typical cell size, s_0 , and the dispersion of the Gaussian random field assumed for the RM structure, σ . The power-law structure function contains a third parameter, the exponent of the power-law, m . T91 suggests $m = 2$ in his analysis, but other values may apply in different sources. Since for the power-law model we have $p \propto \lambda^{-4/m}$ (T91), we can estimate m for sources with measured polarised fluxes at widely spaced wavelengths. Fitting this prediction to the observations of a small sample of radio galaxies observed at 1.4, 4.8 and 8.4 GHz (Akujor & Garrington, 1995), we find $1 \leq m \leq 4$. In the following we use $m = 4$ and $m = 2$.

5.2 Dispersion of rotation measure

For a given set of model parameters s_0 and σ we calculate from equations (3), (5) and (7) the expected observed RM dispersion, σ_{RM} , for each source. We compare this model prediction with the observed value of σ_{RMz} and calculate the χ^2 -deviation of the model for each source. We then minimise the overall χ^2 -value for the entire sample by varying s_0 and σ . In the following we do not aim for a formal best-fitting model. We are only interested in the general form of models that are consistent with the data.

Implicitly we assume here that both model parameters do not vary with redshift and are the same for all sources. The expressions for σ_{RMz} then lead to $\sigma_{\text{RMz}} \sim 0$ for $t < s_0$ and $\sigma_{\text{RMz}} \sim \sigma$ for

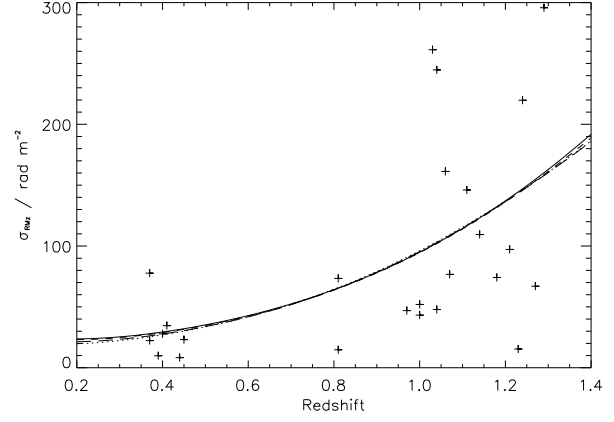


Figure 13. Best fitting models for constant dispersion, σ , and varying s_0 . Symbols show the data for our sample. Solid line: Quadratic structure function. Short-dashed line: Gaussian autocorrelation function. Dotted line: Power-law autocorrelation function with $m = 2$. Long-dashed line: Power-law autocorrelation function with $m = 4$. Model parameters are summarised in Table 11.

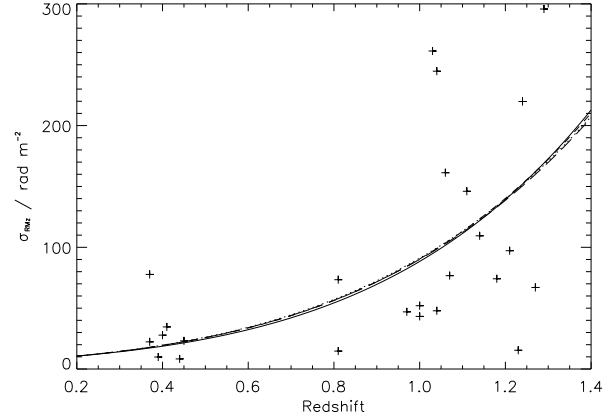


Figure 14. Same as Figure 13, but for constant s_0 and varying dispersion, σ . Model parameters are summarised in Table 11.

$t > s_0$ with a very steep rise in between. Since t increases as z increases, the very rapid transition of σ_{RM} from zero to σ must occur at some finite redshift. As Figure 13 shows, our data are not consistent with this behaviour. Incidentally, the usually assumed model of B66 would predict the same behaviour of σ_{RM} as the models of T91 with constant σ and s_0 discussed here. Thus our data are inconsistent with this model.

Given our data, clearly either s_0 or σ or both must vary with redshift. Therefore we introduce a third model parameter by setting either $\sigma = \text{const.}$ and $s_0 = s_{z=0}(1+z)^\mu$ or, alternatively, $s_0 = \text{const.}$ and $\sigma = \sigma_{z=0}(1+z)^\mu$.

Figures 13 and 14 show the model results in comparison with our observations. Note here that our models cannot fit all data points. However, the plots indicate that all of the models are roughly consistent with the data and that either the dispersion, σ , or the typical cell size, s_0 , or both must be strong functions of redshift (see Table 11). None of the models discussed here fits the data significantly better than the others. In fact, the model parameters are quite similar between the models. Therefore measurements of

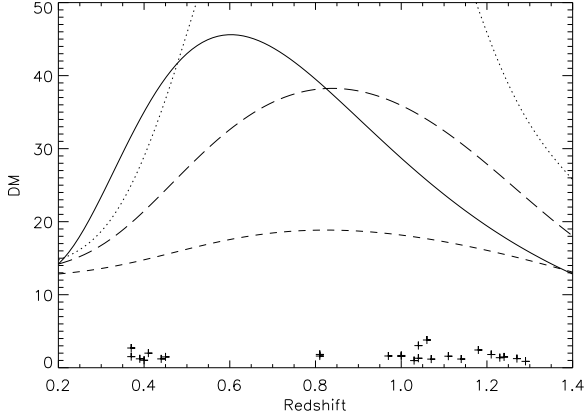


Figure 15. Model predictions for the depolarisation between 1.4 GHz and 4.8 GHz compared with our observations. All models assume a constant dispersion σ and a varying typical cell size s_0 . See Table 11 for details of the model parameters. Solid line: Power-law autocorrelation function with $m = 2$. Dashed line: Same as solid line, but for $m = 4$. Dot-dashed line: Gaussian autocorrelation function. Dotted line: Quadratic structure function.

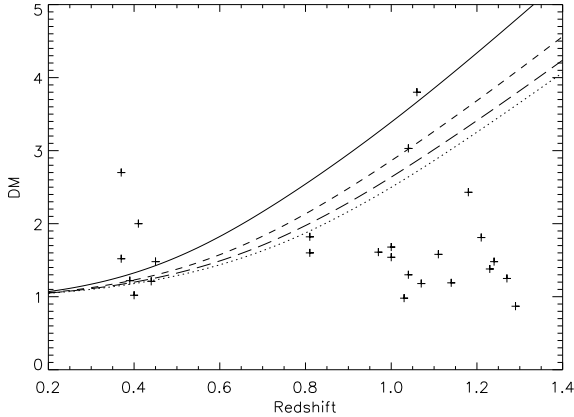


Figure 16. As Figure 15, but for constant s_0 and varying σ .

σ_{RMz} alone do not rule out any of the models. However, it is also clear that a model varying both parameters σ and s_0 with redshift will not provide a significantly improved fit.

5.3 Depolarisation

From equations (3), (5) and (7) we can also derive model predictions for the polarised flux at our two observing frequencies, 1.4 GHz and 4.8 GHz. The ratio of the two provides us with a model estimate of the depolarisation, DM , which we compare with our observations. We use the best-fitting model parameters of the previous Section, summarised in Table 11.

Figure 15 demonstrates that models with a variation of the typical cell size, s_0 , fail to explain the observations. The expected depolarisation significantly exceeds the observed values in all cases. Although these models provide adequate fits to the observed dispersion of the rotation measure, they do not predict the correct behaviour of the percentage polarisation as a function of observing frequency. Models with a constant cell size s_0 , but varying disper-

X, Y	r_{XY}	Student-t
DM_z, z	0.68	6.1
DM_z, P	0.49	3.8
DM_z, D	-0.23	-1.6

Table 12. Spearman Rank coefficients for the correlations between depolarisation, DM_z and the fundamental parameters. The depolarisation is now adjusted using the best-fitting model with a power-law autocorrelation function with $m = 4$. Note that the coefficients are given for depolarisation averaged over the entire source.

sion σ provide a better description of the observations (Figure 16). The depolarisation predicted by all models at high redshifts is still somewhat higher than that observed. However, models for which the dispersion of the rotation measure is a strong function of redshift are clearly preferred compared to those with a varying typical cell size.

We find that our data are reasonably described by a model assuming a power-law autocorrelation function with exponent $m = 4$ and a dispersion varying with redshift as $\sigma = 5.1(z+1)^{4.6} \text{ rad m}^{-2}$. We now use this model instead of the model proposed by B66 to adjust the measured depolarisation of our sources to the common redshift $z = 1$. The adjusted values DM_z show a strong correlation with redshift and a weaker correlation with radio luminosity (see Table 12). If the observed depolarisation of our sources is caused by small-scale structure in a Faraday screen local to the sources, then we would expect both σ_{RMz} and DM_z to correlate with redshift. In Section 3 we found only σ_{RMz} to show this trend, but not DM_z . The results of this Section suggest that the depolarisation model of B66 used in Section 3 is inadequate in describing our observations. For more accurate models we indeed find that both σ_{RMz} and DM_z correlate with redshift. This result strengthens our conclusion in Section 4.3 that the predominant effect changing the polarisation properties of our sources as a function of redshift is the increasing disorder in the structure of the magnetic field in the local Faraday screen of the sources. This decrease in the order of the magnetic fields is reflected in the strong increase in the dispersion of the rotation measure fluctuations in the Faraday screens, σ , with redshift. The change with redshift in the ‘true’ dispersion, σ , gives rise to the behaviour of the observed dispersion, σ_{RMz} , and the observed depolarisation, DM_z .

6 SUMMARY AND CONCLUSIONS

In this paper we investigate in detail radio observations of a sample of 26 extragalactic radio sources of type FR II. The original observations and data reduction are discussed in G04. The observed spectral index, α , the structure of the rotation measure, RM , and depolarisation, DM , of our sources provide us with information on the conditions in the Faraday screens local to the sources.

We first adopt the cosmological redshift, the low frequency radio luminosity and the physical size of our sources as the ‘fundamental’ parameters. We find that the radio spectral index shows no significant correlations with any of the fundamental parameters. The same holds for the rotation measure. The latter result is consistent with our suggestion in G04 that most of the rotation of the plane of polarisation occurs in our Galaxy. On smaller scales the difference of the rotation measure between the two lobes of each source, dRM_z , and the dispersion of the rotation measure, σ_{RMz} , both correlate with redshift and with each other. Thus we conclude

that the variations of RM on small scales is caused by a Faraday screen local to the source. The redshift correlations also imply that the properties of these local Faraday screens change as a function of cosmic epoch. There is no independent correlation of dRM_z or σ_{RMz} with radio luminosity or source size.

The small-scale structure of the rotation measure gives rise to the measured depolarisation of the sources. We initially use the model of B66 for the Faraday screens to convert from the measured DM to DM_z , which we would measure if all our sources were located at the same redshift $z = 1$. The redshift dependence of dRM_z and particularly σ_{RMz} should lead to a similar correlation of DM_z with z . However, although such a correlation is present in our data, it is not significantly stronger than the independent correlation of DM_z with radio luminosity. We argue in Section 5 that the model of B66 is inadequate for describing our data and weakens the correlation between DM_z and redshift. We do not find an anti-correlation of depolarisation measure with size. Some previous studies (Strom 1973; Strom & Jägers 1988; P89; Best et al. 1999; Ishwara-Chandra et al. 1998) find such an anti-correlation while another study does not (Dennett-Thorpe, 1996). In most cases where there is a contradiction between our result and those presented in the literature, the differences can probably be attributed to different telescope resolutions and/or different observing frequencies. However, in the case of P89 and (Dennett-Thorpe, 1996) we have no ready explanation for the disagreement.

We also study the asymmetries between the two lobes of our sources and connections between different kinds of asymmetries. The results are somewhat inconclusive, but seem to favour relativistic beaming of the radio emission of the hotspots as the cause for the observed asymmetries.

We initially employ the commonly used model of B66 for the Faraday screens affecting the polarisation properties of our sources. However, as T91 points out, this ‘standard’ model only applies for observations in which the structure of the magnetic field of the Faraday screen is not resolved. We therefore use the more sophisticated models by T91 to derive estimates for σ_{RMz} and DM_z which we then compare with our observations. We find that only models for which the dispersion of the distribution of RM in the Faraday screens is a strongly increasing function of redshift can successfully explain the observations. All our results therefore point to a decrease in the order of the magnetic field in the Faraday screens with increasing redshift. If the structure of the magnetic field reflects the state of the gas in the source environments, then this finding implies that radio-loud AGN at high redshifts are located in more turbulent environments compared with their low redshift counterparts.

ACKNOWLEDGMENTS

We would like to thank the referee for very helpful comments. JAG thanks PPARC for support in the form of a postgraduate studentship. CRK thanks PPARC for rolling grant support.

References

Akujor C. E., Garrington S. T., 1995, *A&A Supp.*, 112, 235
 Athreya R. M., Kapahi V. K., 1999, in Röttgering H. J. A., Best P. N., Lehnert M. D., eds, *The most distant radio galaxies*. Royal Netherlands Acad. Arts, p. 453
 Barthel P. D., Miley G. K., 1988, *Nat.*, 333, 319

Best P. N., Eales S. A., Longair M. S., Rawlings S., Röttgering H. J. A., 1999, *MNRAS*, 303, 616
 Blundell K. M., Rawlings S., Willott C. J., 1999, *AJ*, 117, 677
 Bridle A. H., Hough D. H., Lonsdale C. J., Burns J. O., Laing R. A., 1994, *AJ*, 108, 766
 Burn B. J., 1966, *MNRAS*, 133, 67, [B66]
 Carilli C. L., Barthel P. D., 1996, *ARA&A*, 7, 1
 Deeming T. J., 1964, *MNRAS*, 127, 493
 Dennett-Thorpe J., 1996, PhD thesis, University of Cambridge
 Eales S., Rawlings S., Law-Green D., Cotter G., Lacy M., 1997, *MNRAS*, 291, 593
 Efstathiou G., Fall S. M., 1984, *MNRAS*, 206, 453
 Fanaroff B. L., Riley J. M., 1974, *MNRAS*, 167, 31
 Garrington S. T., Conway R. G., 1991, *MNRAS*, 250, 198
 Gilbert G. M., Riley J. M., Hardcastle M. J., Croston J. H., Pooley G. G., Alexander P., 2004, *MNRAS*, 351, 845
 Goodlet J. A., Kaiser C. R., Best P. N., Dennett-Thorpe J., 2004, *MNRAS*, 347, 508, [G04]
 Hales S. E. G., Masson C. R., Warner P. J., Baldwin J. E., 1990, *MNRAS*, 246, 256
 Harvanek M., Stocke J. T., 2002, *AJ*, 124, 1239
 Hill G. J., Lilly S. J., 1991, *ApJ*, 367, 1
 Ishwara-Chandra C. H., Saikia D. J., Kapahi V. K., McCarthy P. J., 1998, *MNRAS*, 300, 269
 Ishwara-Chandra C. H., Saikia D. J., McCarthy P. J., van Breugel W. J. M., 2001, *MNRAS*, 323, 460
 Kaiser C. R., 2000, *A&A*, 362, 447
 Kaiser C. R., Alexander P., 1999, *MNRAS*, 302, 515
 Kaiser C. R., Dennett-Thorpe J., Alexander P., 1997, *MNRAS*, 292, 723
 Kapahi V. K., 1989, *AJ*, 97, 1
 Kronberg P. P., Conway R. G., Gilbert J. A., 1972, *MNRAS*, 156, 275
 Lacy M., Rawlings S., Hill G. J., Bunker A. J., Ridgway S. E., Stern D., 1999, *MNRAS*, 308, 1096
 Laing R. A., Riley J. M., Longair M. S., 1983, *MNRAS*, 204, 151
 Leahy J. P., 1987, *MNRAS*, 226, 433
 Leahy J. P., Pooley G. G., Riley J. M., 1986, *MNRAS*, 15, 753
 Liu R., Pooley G. G., 1991a, *MNRAS*, 249, 343
 Liu R., Pooley G. G., 1991b, *MNRAS*, 253, 669
 Longair M. S., Riley J. M., 1979, *MNRAS*, 188, 625
 Macklin J. T., 1982, *MNRAS*, 199, 1119
 McCarthy P. J., Spinrad H., van Breugel W., 1995, *ApJ Supp.*, 99, 27
 Morris D., Tabara H., 1973, *P. As. J.*, 25, 295
 Neeser M. J., Eales S. A., Duncan-Green J., Leahy J. P., Rawlings S., 1995, *ApJ*, 451, 76
 Onuora L. I., 1989, *Ap. & Sp. Sci.*, 162, 349
 Pedelty J. A., Rudnick L., McCarthy P. J., Spinrad H., 1989, *AJ*, 97, 647, [P89]
 Pentericci L., van Reeve W., Carilli C. L., Röttgering H. J. A., Miley G. K., 2000, *A&A Supp.*, 145, 121
 Pooley D. M., Waldram E. M., Riley J. M., 1998, *MNRAS*, 298, 637
 Riley J. K., Hobson M. P., Bence S. J., 1997, *Mathematical methods for physics and engineering*. Cambridge University Press
 Singal A. K., 1988, *MNRAS*, 233, 87
 Singal A. K., 1993, *MNRAS*, 263, 139
 Strom R. G., 1973, *A&A*, 25, 303
 Strom R. G., Jägers W. J., 1988, *A&A*, 194, 79
 Tribble P. C., 1991, *MNRAS*, 250, 726, [T91]
 Véron M. P., Véron P., Witzel A., 1972, *A&A*, 18, 82

Wold M., Lacy M., Lilje P. B., Serjeant S., 2000, MNRAS, 316,
267